Self-Improving Anode for Lithium-Ion Batteries Based on Amorphous to Cubic Phase Transition in TiO2 Nanotubes

ARTICLE *in* THE JOURNAL OF PHYSICAL CHEMISTRY C · JANUARY 2012

Impact Factor: 4.77 · DOI: 10.1021/jp210793u

14 AUTHORS, INCLUDING:

Elena V Shevchenko
Argonne National Laboratory
90 PUBLICATIONS **9,353** CITATIONS
SEE PROFILE

Nada M Dimitrijevic
Argonne National Laboratory
125 PUBLICATIONS **4,260** CITATIONS
SEE PROFILE

Christopher S Johnson
Argonne National Laboratory
69 PUBLICATIONS **3,635** CITATIONS
SEE PROFILE

Tijana Rajh
Argonne National Laboratory
176 PUBLICATIONS **7,503** CITATIONS
SEE PROFILE

THE JOURNAL OF PHYSICAL CHEMISTRY C

ARTICLE

pubs.acs.org/JPCC

Self-Improving Anode for Lithium-Ion Batteries Based on Amorphous to Cubic Phase Transition in TiO_2 Nanotubes

Hui Xiong,[†] Handan Yildirim,[†] Elena V. Shevchenko,[†] Vitali B. Prakapenka,[⊥] Bonil Koo,[†] Michael D. Slater,[‡] Mahalingam Balasubramanian,[§] Subramanian K. R. S. Sankaranarayanan,[†] Jeffrey P. Greeley,[†] Sanja Tepavcevic,[†] Nada M. Dimitrijevic,[†,‡] Paul Podsiadlo,[†] Christopher S. Johnson,[*,‡] and Tijana Rajh[*,†]

[†]Center for Nanoscale Materials, [‡]Chemical Sciences and Engineering, and [§]Advanced Photon Source, Argonne National Laboratory, 9700 S. Cass Avenue, Argonne, Illinois 60439, United States

[⊥]Center of Advanced Radiation Sources, University of Chicago, Chicago, Illinois 60637, United States

Supporting Information

ABSTRACT: We report an electrochemically driven transformation of amorphous TiO_2 nanotubes for Li-ion battery anodes into a face-centered-cubic crystalline phase that self-improves as the cycling proceeds. The intercalation/deintercalation processes of Li ions in the electrochemically grown TiO_2 nanotubes were studied by synchrotron X-ray diffraction and absorption spectroscopies along with advanced computational methods. These techniques confirm spontaneous development of a long-range order in amorphous TiO_2 in the presence of high concentration of Li ions (>75%). The adopted cubic structure shows long-term reversibility, enhanced power with capacity approaching the stochiometry of $Li_2Ti_2O_4$. The anode shows also superior stability over 600 cycles and exhibits high specific energy (~200 W h $kg_{electrode}^{-1}$) delivered at a specific power of ~30 kW $kg_{electrode}^{-1}$. The TiO_2 anode in a full Li-ion cell with a $LiNi_{0.5}Mn_{1.5}O_4$ cathode operates at 2.8 V and demonstrates the highest (~310 mA h/g) reversible specific capacity reported to date. Our conceptually new approach fosters the ability of amorphous nanoscale electrodes to maximize their capacity in *operando*, opening a new avenue for synthesis of safe and durable high-power/high-capacity batteries.

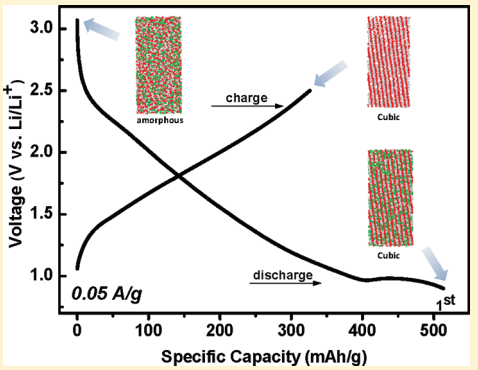

INTRODUCTION

Limited energy resources and the growing demand to decrease greenhouse gas emissions have intensified research on carbon-free energy sources. Batteries that store high-energy densities play a large role in the implementation of green energy technologies and non-petroleum vehicular mobility. Rechargeable Li-ion batteries offer the highest energy density of any present battery technology[1] and are expected to provide a solution for our future energy-storage requirements. However, Li-ion batteries still have a number of limitations, such as capacity loss during prolonged cycling due to phase transitions that lead to detrimental volume changes in the electrode materials.[2] This can cause local atomic rearrangements, blocking the diffusion of Li ions and creating high electrode overpotentials and capacity degradation. In addition, Li-ion batteries that are charged too quickly may lead to Li plating at the graphite, the dominant anode in lithium-ion batteries, causing a safety hazard that in the worst case scenario could lead to thermal runaway, cell rupture, and explosion. Use of chemically inert anode materials such as metal oxides with lithiation voltages positive of Li deposition compared to graphite while maintain high reversible capacity is a promising solution to these problems.

Titania (TiO_2) is one of the few metal oxide materials that intercalates Li ions at reasonably low voltage (~1.5 V vs Li/Li^+) as an alternative to graphite.[3] The first attempts at using TiO_2 as a durable and safe anode were focused on microcrystalline rutile, anatase, and TiO_2(B).[4] These electrodes showed moderate capacities (the maximum Li uptake of 0.5 Li/Ti for anatase and TiO_2(B) and no activity for rutile)[4] due to the limited room temperature reactivity and conductivity at microscale. Recently, nanosized TiO_2 electrodes demonstrated capacities with stoichiometries up to ~0.5−0.7 Li/Ti due to enhanced intercalation kinetics and large surface area;[5] however, prolonged cycling caused loss of capacity independent of the crystalline modification.[3]

Herein, we report a new approach for creating high-capacity/high-power electrodes starting from amorphous TiO_2NTs that undergo irreversible phase transformation by self-organization upon electrochemical cycling with Li^+. Self-organization of materials during electrochemical cycling has never been reported before and could be an easy general approach for synthesis of new crystalline forms of materials for electrodes in Li-ion batteries.

EXPERIMENTAL METHODS

TiO_2 nanotubes were synthesized by electrochemical anodization. Pure titanium thin foil (0.0127 mm, 99.8%, Alfa Aesar)

Received: November 9, 2011
Published: December 22, 2011

was cleaned by acetone following an isopropyl alcohol rinse before anodization. The back of the Ti foil was protected by nail polish to ensure uniform current distribution. The anodization was carried out in a two-electrode cell with Ti metal as the working electrode and a Pt mesh as the counter electrode under constant potentials (15−30 V) at room temperature using electrolytes of formamide with 0.8 wt % ammonium fluoride (Aldrich) and 5 vol % DI water. The as-anodized samples were ultrasonically cleaned in DI water for 30 s. All amorphous TiO_2NT samples were vacuum-annealed at 110 °C overnight before assembly in electrochemical cells. The anatase TiO_2NT samples were prepared by annealing as-prepared TiO_2NT under O_2 at 450 °C for 4 h. Annealing of phase-transformed TiO_2NT under the same condition does not result in anatase nanotubes.

The $LiNi_{0.5}Mn_{1.5}O_4$ spinel[6] cathode materials were prepared by solid-state reactions as follows: quantities of Li_2CO_3 and $Ni_{0.25}Mn_{0.75}CO_3$ (prepared by coprecipitation) to achieve the desired stoichiometry were ground together in an agate mortar until visually homogeneous. The mixture was initially fired in a muffle furnace at 550 °C for 12 h, reground, and then calcined at 850 °C for 12 h and allowed to slowly cool to ambient temperature. Structures were verified by powder XRD, and the relative metals contents were measured by ICP-OES and found to be the target compositions within the error of the determination. Electrode films were cast from slurries in *N*-methyl-2-pyrrolidone containing the active material (82% w/w), carbon black (4% w/w, Cabot XC72), graphite (4% w/w, Timcal SFG-6), and poly(vinylidene difluoride) (10% w/w; Kynar KF1120) using doctor blade or spin-casting techniques.

Li half-cells were assembled in coin-type cells (Hohsen 2032) with a Li metal foil as the negative electrode, microporous polyolefin separators (Celgard 2325), and 1.2 M $LiPF_6$ in ethylene carbonate/ethyl methyl carbonate (3:7 weight ratio) electrolyte (Tomiyama). Half-cells were cycled galvanostatically at varying currents between 2.5 and 0.9 V vs Li/Li^+ using an automated Maccor battery tester at ambient temperature. Li-ion full cells were assembled in the same manner as half-cells with a $LiNi_{0.5}Mn_{1.5}O_4$ cathode. Li-ion full cells were cycled galvanostatically between 2 and 3.5 V. Electrodes removed from cells for analysis were thoroughly washed with dry dimethyl carbonate (Aldrich) and allowed to dry under inert atmosphere. All cell assembly and disassembly operations were performed in a He-filled dry glovebox (oxygen level <2 ppm). The actual mass of the TiO_2 nanotube films was determined by peeling off the nanotube film from Ti substrate using adhesives and measuring the weight difference. The remaining substrate was examined by SEM to make sure that no residual TiO_2 nanotube was left on the substrate.

X-ray diffraction measurements were performed at beamline 13-ID-D of GSECARS at the Advanced Photon Source (APS) at Argonne National Laboratory. The X-ray beam (37 keV energy, corresponding to X-ray wavelength of λ = 0.3344 Å) was focused to a 2 μm diameter spot with a Kirkpatrick-Baez mirror system. The distance and tilting of the MAR165-CCD detector were calibrated using a CeO_2 standard. Charged TiO_2NT samples were prepared by stripping nanotube films from Ti support onto Kapton tape and sandwiching with additional Kapton tape. Electrochemically lithiated TiO_2NT samples were scratched off and sealed inside a 3 mm diameter hole in a piece of aluminum foil by sealing Kapton sheet to the foil using epoxy. All procedures were carried out in a He atmosphere glovebox. Simulations of XRD patterns were carried out using CrystalMaker (CrystalMaker Software, Ltd.). Simulations of XRD (227 space group) assumed the same sites occupied by Li and Ti atoms with 0.5 site occupancy.

Scanning electron microscopy (SEM) images were recorded with a JEOL JSM-7500F field emission SEM operating at 10 kV. High-resolution electron transmission microscopy (HRTEM) images and electron diffraction (ED) were obtained using an FEI Tecnai F30 microscope equipped with a field emission gun operated at 300 kV. TEM samples were prepared by scratching cycled TiO_2NT samples from Ti support onto a carbon-coated copper TEM grid (ultrathin carbon film on holey carbon support film, 400 mesh, Ted Pella Inc.).

Molecular dynamics (MD) simulations are performed using the DLPOLY MD package,[7] and electronic structure calculations are within Vienna *ab initio* simulation package (VASP).[8,9] Our MD simulations utilize the shell potential model in which the polarizable ion consists of two particles—core and shell—that share the ion's charge and are connected via a spring constant. The atoms are treated as point particles and interact via long-range Coulomb forces and short-range interactions. The short-range interactions are represented by the Buckingham potential, which is described by parametrized functions fitted to reproduce the structure and energetics of Li−Ti−O system. In all MD simulations, the system size of 4320 atoms is used. The calculations span a temperature range of 850−1400 K, and statistics are typically collected from 1 ns simulations with a time step of 0.2 fs. To gather enough statistics, the calculations are performed at high temperatures, and the necessary information is extrapolated to low temperature. Density functional theory (DFT) calculations are performed using GGA-PBE.[10] The cubic structure is made of 64 atoms, while the amorphous cell is constructed using 96 atoms. The initial structure of the amorphous cell for DFT calculations is obtained from the equilibrated configurations generated from the MD simulations. At least three different amorphous configurations were simulated to ensure that the results are not biased by the initial starting configuration. For all the systems, we allow both the cell shape to change and ions to relax. The calculations are performed using 550 eV energy cutoff and 5 × 5 × 5 k-point sampling.

X-ray absorption spectroscopy measurements were performed at the PNC/XSD bending magnet beamline (20-BM-B) of the APS at Argonne National Laboratory. Measurements at the Ti K-edge were performed under transmission mode using gas ionization chambers to monitor the incident and transmitted X-ray intensities. A third ionization chamber was used in conjunction with a Ti-foil standard to provide internal calibration for the alignment of the edge positions. The incident beam was monochromatized using a Si (111) double crystal fixed exit monochromator. Harmonic rejection was accomplished using a rhodium-coated mirror. The charged samples were prepared by stripping NT films onto Kapton tape. The discharged samples were stripped onto Kapton tape in a He dry glovebox and attached to a He-filled, sealed holder. The reference standards were prepared by spreading thin, uniform layers of powders on Kapton tape and stacking a few layers to attain the desired absorption step height. Each spectrum was normalized using data processing software package IFEFFIT.[11] Alignment of each sample reference spectrum with respect to Ti standard spectrum is within the range of ±0.03 eV.

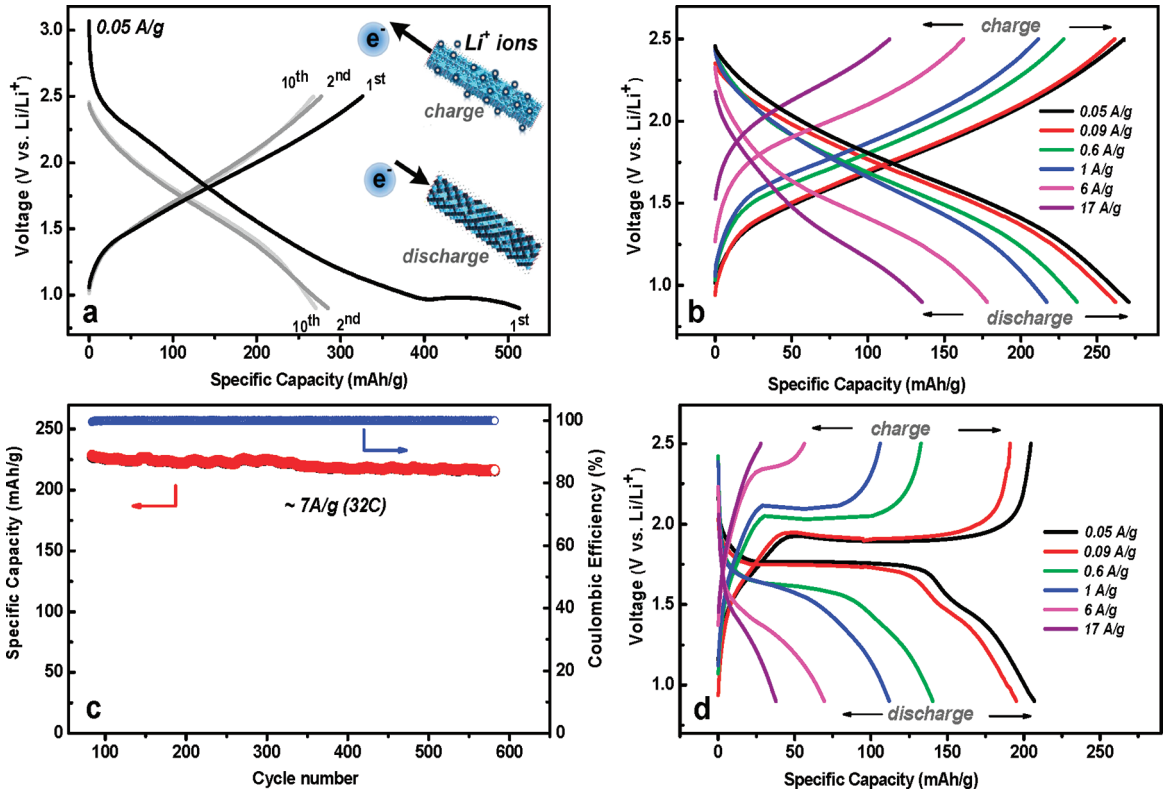

Figure 1. Electrochemical characterization of TiO_2NTs. (a) Charge/discharge galvanostatic curves of amorphous TiO_2NT (2.5 μm long and 65 nm o.d.) electrode. Ti octahedra are light blue, and Li octahedra after intercalation are dark blue. Rate capabilities of TiO_2NT after phase transition (10th cycle) (b) and anatase TiO_2NT (d) at different current rates. (c) Cycling performance of amorphous-to-crystalline TiO_2NT electrode. Red circle: discharge; black circle: charge; blue circle: Coulombic efficiency. The TiO_2NT electrode had been cycled at a wide range of current densities prior to the cycle life test.

RESULTS AND DISCUSSION

Recently, we have shown that amorphous TiO_2NT can be used to reversibly cycle Na ions[12] with percolation pathways facilitating the diffusion of ions.[13,14] Thus, we have chosen amorphous nanoscale TiO_2 as an anode, expecting enhanced diffusion of Li ions. Using electrochemical anodization of Ti foil,[15−18] we synthesized densely packed, vertically oriented amorphous TiO_2 nanotubes (TiO_2NTs) that are electronically connected to the current collector (Supporting Information Figure S1a). This electrode design facilities efficient electron transport while eliminating the need for conductive carbon additives and binders typically used in electrodes that can alter their long-term stability.[19] Previously, Lin et al. have reported near-theoretical capacity of amorphous TiO_2 thin film (800 nm) grown by reactive ballistic deposition;[20] however, they also noticed that the lithiation of copper current collector contributed to the overall capacity. Whereas there are several reports of electrochemical properties associated with Li insertion into amorphous TiO_2 nanotube arrays,[18,21,22] the information regarding the effect of the intrinsic properties of the amorphous nanotubes on their electrochemical performance is scarce.

When amorphous TiO_2NTs are used as electrodes in a lithium half-cell, a monotonic linear decreasing voltage is observed during the first discharge (Li^+ insertion), followed by a characteristic "hump" at ~1.1 V vs Li/Li^+. The existence of the "hump" indicates irreversible phase transition (Figure 1a). The specific capacity of the first charge (Li^+ deinsertion) is close to the theoretical value of 335 mA h/g, assuming 1 Li per 1 TiO_2, while a high capacity (520 mA h/g, 1.55 Li per 1 TiO_2) observed at the first discharge can be attributed to the reduction of surface OH groups and residual surface H_2O by Li atoms[23−25] (Supporting Information Figure S3). Therefore, the near theoretical capacity observed in the first cycle previously reported by Bhattacharyya et al.[25] cannot be considered as the reversible capacity as the capacity continues to fade with subsequent cycling due to side reactions with highly reactive reducing species or irreversible distortion of crystalline framework. In this work, however, in subsequent cycles, Li^+ ions reversibly intercalate/deintercalate into TiO_2NTs with specific capacity as high as 271 mA h/g at a rate of C/5 (C/n, discharge the sample in n hours) at room temperature (Figure 1a), which is significantly larger than the highest capacities (170 mA h/g) experimentally observed in anatase or rutile polymorphs of TiO_2.[4,26] This value is also higher than the calculated theoretical value of 250 mA h/g corresponding to the stoichiometry of $Li_{0.75}TiO_2$ for the highest capacity polymorphs.[27]

Our observation of reversible capacity in phase-transformed nanotube electrodes that exceeds the theoretically predicted values for any of the TiO_2 polymorphs must be the consequence of a different intercalation mechanism, different structure, or the presence of different intercalation sites in nanotube electrodes compared to traditional bulk electrodes. The rate capability study confirms superior diffusion of Li ions in phase-transformed TiO_2NT electrode compared to anatase TiO_2NT electrode obtained by annealing of amorphous TiO_2NT at 450 °C (Figure 1b,d). This was especially apparent at high rate (17 A/g) when significantly

dx.doi.org/10.1021/jp210793u |J. Phys. Chem. C 2012, 116, 3181–3187

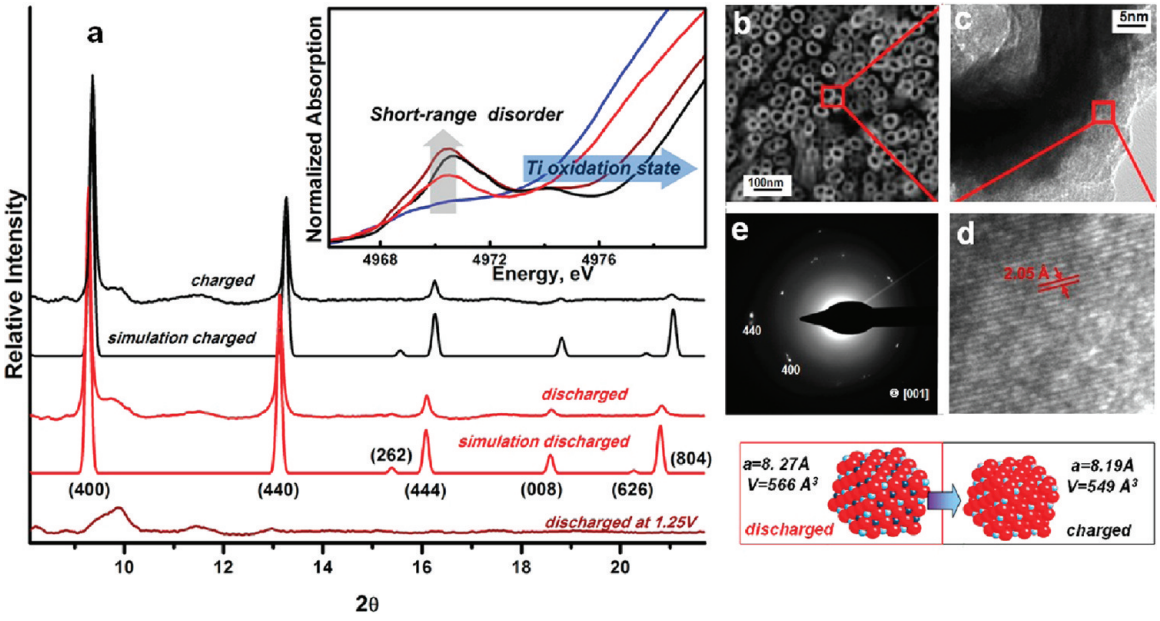

Figure 2. Structural characterization of amorphous TiO_2NTs at different stages of cycling. (a) Synchrotron XRD measurements at the stages of discharged to 1.25 V vs Li/Li^+ (brown curve), discharged to 0.9 V (red), followed by charged to 2.5 V (black). Inset: pre-edge feature in the Ti K-edge XANES for the same samples. T_2O_3 spectrum (blue) is shown for reference. (b−e) SEM and TEM images of charged TiO_2NTs. (b) SEM image of charged TiO_2NTs. (c) Individual nanotube after cycling. (d) HRTEM image at a region of the same tube (red square) showed fringes corresponding to a lattice spacing of 2.05 Å. (e) Selected area electron diffraction (SAED).

higher capacity (135 mA h/g) was preserved in charging of phase-transformed TiO_2NT within 26 s compared to 38 mA h/g of the same tubes converted to anatase TiO_2 form. This capacity at high rate is comparable to the theoretical capacity (175 mAh/g) of $Li_4Ti_5O_{12}$,[3] currently considered as a safe alternative to graphite anode. At this high rate, phase-transformed TiO_2NT electrode demonstrated high specific energy (~200 W h $kg_{electrode}^{-1}$) delivered at an exceptionally high specific power (~30 kW $kg_{electrode}^{-1}$), based on TiO_2NT electrode weight alone. Current rechargeable Li batteries have higher energy but lower power (~150 W h kg_{cell}^{-1} and ~1 kW kg_{cell}^{-1}) than electrochemical capacitors (~5 W h kg_{cell}^{-1} and ~10 kW kg_{cell}^{-1}).[28] The phase-transformed TiO_2NT electrode thus combined advantages from both devices to exhibit high energy and meanwhile deliver high power. Moreover, the capacity of the TiO_2NT self-improved with cycling at fast rate (~32 C) within 60 cycles with Columbic efficiency higher than 99%.[12] In contrast, similar experiments on anatase NT electrodes show a slight capacity decrease in fast charge−discharge cycles. These results suggest that intercalation/deintercalation of Li^+ ions in phase-transformed TiO_2NT initiates the development of a new structure that is much better suited for intercalation of Li^+ ions. Even at the fast cycling rate of 2C the sample preserves reversible capacity and operates with ~100% Coulombic efficiency for ~600 cycles (Figure 1c).

We used a combination of analytical techniques based on synchrotron X- ray spectroscopies and computational techniques to understand the structural transformation of amorphous TiO_2NTs at the atomic scale. XRD analysis showed no structural change was induced upon cycling of amorphous TiO_2NTs above ~1.1 V (the potential at the shoulder of the first discharge) (Figure 2a). However, cycling at potentials below 1.1 V demonstrated the formation of a new crystalline material with high degree of symmetry where Ti and Li are randomly distributed among all octahedral sites in a nearly ideal cubic closed packed oxygen array. This crystalline transformation is accompanied by dramatic decrease of the oxidation state of Ti when potential was changed only from 1.25 to 0.9 V (Figure 2a; inset: brown and red curve, respectively), indicating dramatic increase in the capacity in this potential range.

It should be noted that while XRD indicates development of a long-range order immediately after the first discharge. On the other hand, the pre-edge feature in the Ti K-edge X-ray Absorption near-edge structure (XANES) (symmetry forbidden 1s−3d transition in Ti that gains intensity with decreasing centrosymmetry)[29] shows that the short-range order expected for fully ordered octahedral system is not developed with cycling (Figure 2a, inset). Although oxidation state of Ti in lithiated samples approaches that of Ti_2O_3 (Figure 2a, inset), the short-range order does not evolve. High-resolution transmission electron microscopy (HRTEM) analysis revealed a well-defined 2.05 Å crystal lattice spacing (Figure 2d), corresponding to the newly emerged (400) plane of the charged sample shown in XRD. Also, selected-area electron diffraction (SAED) pattern on the tubes indicated (400) and (440) crystal planes of the cubic phase (Figure 2e, Supporting Information Figure S2).

The cell parameter of the discharged unit cell of 8.27 Å is somewhat smaller than the one previously reported for chemically prepared bulk $Li_2Ti_2O_4$ (a = 8.376 Å)[30] of the same symmetry; however, it is significantly smaller than that of the spinel phase with stochiometry of $LiTi_2O_4$ where Li occupies tetrahedral sites expanding the unit cell to 8.403 Å.[30] We note that our geometric optimization using DFT calculations gives an optimized lattice constant of 8.27 Å, suggesting a good balance of electrostatic forces (Supporting Information Figure S4a). Moreover, investigation of the samples at different stages of charge shows a linear decrease of the crystal unit cell with decreasing content of Li, suggesting that there is no transition through a spinel phase with decreasing Li content, whereby Ti and Li form

dx.doi.org/10.1021/jp210793u |J. Phys. Chem. C 2012, 116, 3181–3187

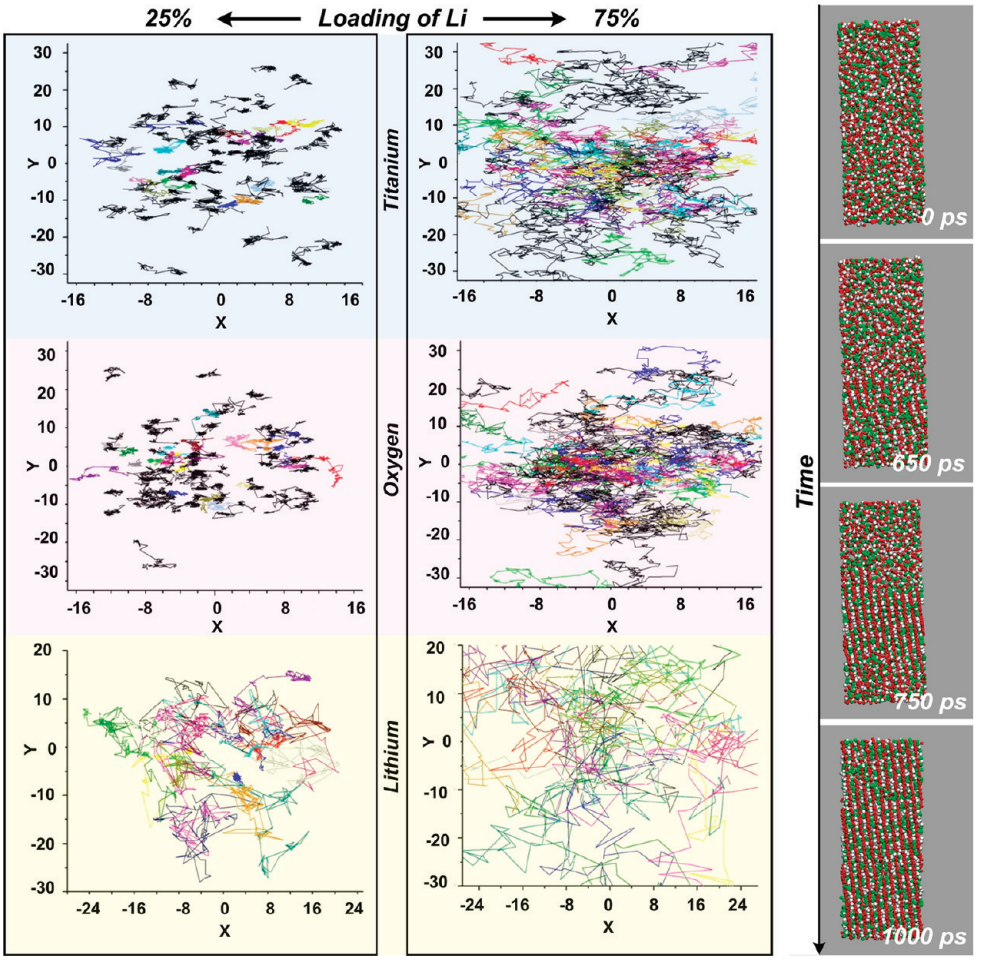

Figure 3. Ionic transport in amorphous TiO_2 as a function of Li stoichiometry. Evolution of the cubic structure from amorphous TiO_2 containing 100% Li ions with time is shown on the right (red spheres: O; green spheres: Li; white spheres: Ti).

a solid solution between charged and discharged states. The small 3% volume change between discharged and charged state does not seem to affect morphology and long-term stability of TiO_2NTs, and the sample preserves capacity and unperturbed morphology (Figure 1c, Supporting Information Figure S1) for ~600 cycles (the extent of our measurement).

MD simulations suggest that atomic diffusivity in the lithiated amorphous TiO_2 structure depends strongly on the lithium content (Figure 3). We find that diffusion coefficients of Ti and O in amorphous TiO_2 having low concentrations of Li are fairly small, comparable to those in other titania polymorphs. At high lithiation levels (>75%), however, atomic diffusion of Ti and O becomes significant, suggesting facile rearrangement of atoms in the structure and leading to phase transformation. This rapid kinetic diffusion, in turn, suggests that crystallization to thermodynamically stable phases of similar composition should be possible during initial discharge of the TiO_2 electrodes. Our formation energy analysis also indicates that the cubic structure is energetically more favorable than amorphous titania with the same lithium loading (Supporting Information Figure S7). Indeed, MD simulations for the 100% Li-loaded amorphous TiO_2 composition (Figure 3, Supporting Information video) show evolution of a long-range order, as revealed by the formation of regularly ordered layers of oxygen. These well-defined layers of oxygen are separated by layers of mixed metal (Ti and Li) atoms that are randomly distributed. Note that this layered formation is the same as the cubic phase observed in the experiments. Further simulations performed up to 10 ns do not show increase in short-range ordering, suggesting that the structure should possess stable long-range order but that short-range ordering is kinetically inhibited. For Li concentrations *much lower* than 100%, the lithiated amorphous oxide maintains its disordered structure for the same time and temperature conditions, indicating that the kinetics of this transformation is strongly correlated to the Li:TiO_2 stoichiometry.

We believe that existence of long-range order in the absence of short-range order within layers (chemical disorder) is a key factor in the thermodynamic stability of the delithiated structure. The fact that, in this structure, all layers continue to contain metal atoms, even in the charged state, provides stability and prevents collapse of the delithiated structure. Accordingly, our DFT calculations also show that the optimized structure for the fully delithiated titania preserves cubic symmetry. Our experimental results confirm thermodynamic stability of the cubic phase as annealing of delithiated cubic TiO_2 to high temperatures does not lead to any phase transformation. We believe the preservation of the cubic structure accounts for the high stability and reversibility of the amorphous-to-cubic TiO_2NT electrodes.

Interestingly, previous reports of bulk fcc $Li_2Ti_2O_4$ suggest that this structure cannot be employed for reversible cycling.[31]

dx.doi.org/10.1021/jp210793u |*J. Phys. Chem. C* 2012, 116, 3181–3187

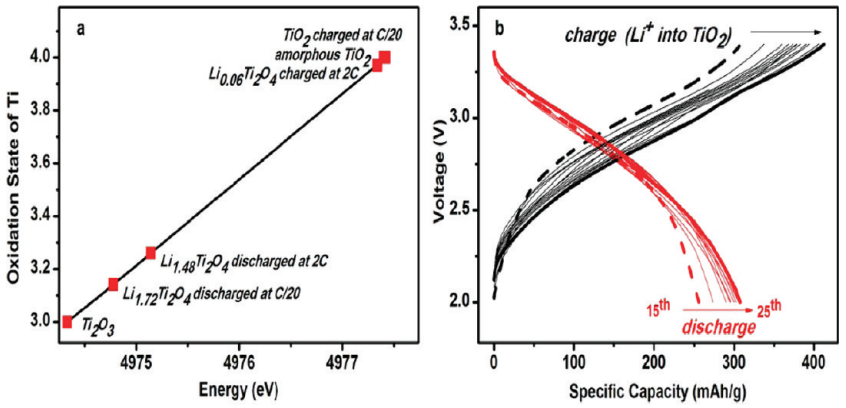

Figure 4. Electrochemical characterization of a TiO_2NT/$LiNi_{0.5}Mn_{1.5}O_4$ cell. (a) Oxidation states of Ti in TiO_2NT electrodes at different charged/discharged states obtained from Ti K-edge XANES. (b) Charge/discharge voltage profile of a TiO_2NT-$LiNi_{0.5}Mn_{1.5}O_4$ battery at ambient temperature cycled a rate of C/15.

It has been shown that chemically synthesized bulk cubic $Li_2Ti_2O_4$ can be oxidized to $Li_{0.1}TiO_2$, but removal of Li^+ results in a defective disordered cubic structure that is virtually unreactive for further Li intercalation.[31] On the other hand, nanoscale architectures obtained in this work by self-organization of amorphous samples show entirely reversible Li insertion/extraction, demonstrating a solid solution mechanism, good Coulombic efficiencies, and confirming facile diffusion of Li ions (Figure 1a). To understand how the diffusion characteristics of lithium in the self-improved cubic structure compare with those in other titania structures, we perform MD simulations of Li ion diffusion in a variety of highly lithiated crystalline and amorphous titania structures, including amorphous, cubic $Li_2Ti_2O_4$ as well as anatase TiO_2 (Figure 3 and Supporting Information Figure S5). Comparison of the trajectories suggests that Li ion transport in fully lithiated samples follows cubic (100% Li) > amorphous (100% Li) > anatase (50% Li), which is consistent with the high reversible capacity observed for the self-improved structure as compared to other titania polymorphs. In fact, calculation of Li ion diffusion in the cubic $Li_2Ti_2O_4$ reveals a remarkably low diffusion activation barrier (0.257 eV; Supporting Information Figure S6) compared to 0.5 eV for anatase,[32] implying that rapid lithiation and delithiation of the cubic 227 structures should be possible during successive discharge/charge cycles. The facile Li diffusion in this cubic structure explains its superior power capability compared to anatase (Figure 1).

This finding supports our XANES measurements that confirm commendable discharging/charging even at fast cycling rate (Figure 4a). We used X-ray absorption spectroscopy (XAS) to follow the change of Ti oxidation state as a function of state of charge. As each reduced Ti center in metal oxide framework is associated with one intercalated ion that screens introduced electrons, measurement of the oxidation state of Ti ions directly reports on specific capacity of the electrode. We see from XANES spectra of Ti K-edge that the oxidation state of discharged phase transformed cubic TiO_2NT at slow rate (C/20) reaches nearly fully reduced state and theoretical capacity as Ti atoms on average achieve oxidation state of 3.14 (corresponding to the stochiometry of $Li_{1.72}Ti_2O_4$). We can see, however, that by cycling at a faster rate of ~2C the electrode's state of charge are consistent with the decreased capacity observed under rate study (Figure 1). At faster rate a higher oxidation state of 3.26 was found for a discharged sample while that of charged sample stays almost unchanged, 3.97. These results indicate that once Li ions are intercalated into TiO_2 host they can efficiently diffuse out during charging process even at fast rate (oxidation state ~4). However, the rate of cycling affects the process of discharge. As diffusion within electrode must be the same during charge and discharge processes, the factor that limits capacity of cubic TiO_2 nanotubes at high rate has to be associated with ion diffusion within bulk electrolyte.

The full potential of self-organization to cubic TiO_2 on nanoscale can be realized when amorphous-to-cubic TiO_2NT anode was coupled with a 5 V spinel ($LiNi_{0.5}Mn_{1.5}O_4$) cathode[33] for testing in a Li-ion full cell configuration. The cell was constructed such that the specific capacity is limited by the mass of TiO_2NT anode. The TiO_2NT/$LiNi_{0.5}Mn_{1.5}O_4$ cell shows an average cell voltage of 2.8 V and exceptionally good specific capacity that improves as the cycling proceeds. The success of this Li-ion cell made by amorphous-to-cubic TiO_2NT anode demonstrates that it maintained the advantage of a Li-ion battery (large output potential) while moved the operating potential at the anode to a higher window, thus avoiding possible safety hazards from Li plating. The specific discharge capacity of the cell of 256 mA h/g improves with cycles and reaches ~310 mA h/g in less than 25 cycles (16 mA/g, C/15) (Figure 4b), which is higher than any reported specific capacity based on TiO_2. The self-improving mechanism in amorphous TiO_2NT was previously attributed to improved availability of transporting Na ions during cycling[12] and in multiwalled carbon nanotubes to increasing number of defect sites and contribution from the substrates.[34] In this work, however, we observe two distinct mechanisms of electrode capacity improvement: (1) in the first cycle when crystalline transformation from amorphous to cubic occurs and capacity improves for ~100 mA h/g and (2) when cubic crystalline electrode is coupled with the transition metal oxide cathode when capacity improves for ~50 mA h/g. We think that the second mechanism is similar to that described for amorphous TiO_2 NT[12] and originates from improved availability of Li ions at electrode surface upon cycling. Both of these new phenomena of self-improving amorphous materials can be very attractive approaches for the preparation of high-performance electrode materials. It is interesting to note that preconditioning of amorphous TiO_2NT to cubic form removed large irreversible capacity in the first cycle, making the electrode suitable for practical applications.

CONCLUSION

It is at the nanoscale that near theoretical capacity and high-power electrodes can be achieved using simple self-organization processes. The electrostatic attraction of electrochemically altered materials provides a strong driving force for the diffusion of a large concentration of transporting ions into amorphous metal oxide frameworks. This consequently leads to ordering of the atomic building blocks, transporting ions, and metal hosts into a crystalline array. Inducing crystallization of nanomaterials *in operando* allows realization of the highest possible electrode capacity by optimizing the balance of electrostatic forces. This study shows that much higher specific capacities can be realized if the system is naturally allowed to choose and optimize its crystalline structure through a process of self-organization and self-improvement. The small diffusion length and large surface area of nanostructures combined with facile ion diffusion in the adopted crystalline structure enable exceptionally fast charging, leading to high-power batteries. Electrochemically induced structural evolution into high-capacity/high-power electrodes provides a powerful modular approach to the design of improved battery materials with programmable physical and chemical properties.

ASSOCIATED CONTENT

Supporting Information. Structural parameters and characterization of TiO_2NT electrodes; MD and DFT simulations. This material is available free of charge via the Internet at http://pubs.acs.org.

AUTHOR INFORMATION

Corresponding Author

*E-mail: cjohnson@anl.gov (C.S.J.); rajh@anl.gov (T.R.).

ACKNOWLEDGMENT

H.X. thanks Dr. J. Zhang (Northwestern University) for help with TEM measurements. The authors gratefully acknowledge Dr. D. Kim and Dr. S. Kang (ANL) for providing cathode materials for full-cell experiments. The authors acknowledge valuable discussions with Dr. J. Vaughey and Dr. W. Lu (ANL). This work and use of the Center for Nanoscale Materials were supported by the U.S. Department of Energy, US DOE-BES, under Contract DE-AC02-06CH11357. XAS Data were collected on the X-ray Operations and Research beamline 20-BM-B at the Advanced Photon Source, Argonne National Laboratory. Use of the Advanced Photon Source was supported by the U.S. Department of Energy, Office of Science, Office of Basic Energy Sciences, under Contract DE-AC02-06CH11357 and NSERC (Canada). Synchrotron XRD data were collected on the X-ray Operations and Research beamline 13-ID-D (GeoSoilEnviroCARS) at the Advanced Photon Source, Argonne National Laboratory. Use of the beamline was supported by the National Science Foundation, Earth Sciences (EAR-0622171), and U.S. Department of Energy, Geosciences (DE-FG02-94ER14466). The authors acknowledge the use of TEM at the Electron Microscopy Facilities at the University of Chicago.

REFERENCES

(1) Tarascon, J. M.; Armand, M. *Nature* **2001**, *414*, 359–367.
(2) Chan, C. K.; Peng, H.; Liu, G.; McIlwrath, K.; Zhang, X. F.; Huggins, R. A.; Cui, Y. *Nature Nanotechnol.* **2008**, *3*, 31–35.
(3) Yang, Z. G.; Choi, D.; Kerisit, S.; Rosso, K. M.; Wang, D. H.; Zhang, J.; Graff, G.; Liu, J. *J. Power Sources* **2009**, *192*, 588–598.
(4) Zachauchristiansen, B.; West, K.; Jacobsen, T.; Atlung, S. *Solid State Ionics* **1988**, *28*, 1176–1182.
(5) Bruce, P. G.; Scrosati, B.; Tarascon, J. M. *Angew. Chem., Int. Ed.* **2008**, *47*, 2930–2946.
(6) Zhong, Q. M.; Bonakdarpour, A.; Zhang, M. J.; Gao, Y.; Dahn, J. R. *J. Electrochem. Soc.* **1997**, *144*, 205–213.
(7) Smith, W.; Forester, T. R. *J. Mol. Graphics* **1996**, *14*, 136.
(8) Kresse, G.; Furthmüller, J. *Comput. Mater. Sci.* **1996**, *6*, 15.
(9) Kresse, G.; Furthmüller, J. *Phys. Rev. B* **1996**, *54*, 11169.
(10) Perdew, J. P.; Burke, K.; Ernzerhof, M. *Phys. Rev. Lett.* **1996**, *77*, 3865.
(11) Newville, M. *J. Synchrotron Radiat.* **2001**, *8*, 322–324.
(12) Xiong, H.; Slater, M. D.; Balasubramanian, M.; Johnson, C. S.; Rajh, T. *J. Phys. Chem. Lett.* **2011**, *2*, 2560–2565.
(13) Paul, H.; Sylvio, I. *J. Phys.: Condens. Matter* **2003**, *15*, R1257.
(14) Heitjans, P.; Tobschall, E.; Wilkening, M. *Eur. Phys. J.: Spec. Top.* **2008**, *161*, 97–108.
(15) Mor, G. K.; Varghese, O. K.; Paulose, M.; Shankar, K.; Grimes, C. A. *Sol. Energy Mater. Sol. Cells* **2006**, *90*, 2011–2075.
(16) Macák, J. M.; Tsuchiya, H.; Schmuki, P. *Angew. Chem., Int. Ed.* **2005**, *44*, 2100–2102.
(17) Tepavcevic, S.; Darling, S. B.; Dimitrijevic, N. M.; Rajh, T.; Sibener, S. J. *Small* **2009**, *5*, 1776–1783.
(18) Ortiz, G. F.; Hanzu, I.; Djenizian, T.; Lavela, P.; Tirado, J. L.; Knauth, P. *Chem. Mater.* **2008**, *21*, 63–67.
(19) Rolison, D. R.; Long, J. W.; Lytle, J. C.; Fischer, A. E.; Rhodes, C. P.; McEvoy, T. M.; Bourg, M. E.; Lubers, A. M. *Chem. Soc. Rev.* **2009**, *38*, 226–252.
(20) Lin, Y.-M.; Abel, P. R.; Flaherty, D. W.; Wu, J.; Stevenson, K. J.; Heller, A.; Mullins, C. B. *J. Phys. Chem. C* **2010**, *115*, 2585–2591.
(21) Fang, H.-T.; Liu, M.; Wang, D.-W.; Sun, T.; Guan, D.-S.; Li, F.; Zhou, J.; Sham, T.-K.; Cheng, H.-M. *Nanotechnology* **2009**, *20*, 225701.
(22) Guan, D.; Cai, C.; Wang, Y. *J. Nanosci. Nanotechnol.* **2011**, *11*, 3641–3650.
(23) Borghols, W. J. H.; Lutzenkirchen-Hecht, D.; Haake, U.; Chan, W.; Lafont, U.; Kelder, E. M.; van Eck, E. R. H.; Kentgens, A. P. M.; Mulder, F. M.; Wagemaker, M. *J. Electrochem. Soc.* **2010**, *157*, A582–A588.
(24) Chen, J. S.; Tan, Y. L.; Li, C. M.; Cheah, Y. L.; Luan, D.; Madhavi, S.; Boey, F. Y. C.; Archer, L. A.; Lou, X. W. *J. Am. Chem. Soc.* **2010**, *132*, 6124–6130.
(25) Das, S. K.; Bhattacharyya, A. J. *J. Phys. Chem. C* **2009**, *113*, 17367–17371.
(26) Hu, Y. S.; Kienle, L.; Guo, Y. G.; Maier, J. *Adv. Mater.* **2006**, *18*, 1421–1426.
(27) Koudriachova, M. V. *J. Solid State Electrochem.* **2010**, *14*, 549–553.
(28) Simon, P.; Gogotsi, Y. *Nature Mater.* **2008**, *7*, 845–854.
(29) Farges, F.; ccedil; ois; Brown, G. E.; Rehr, J. J. *Phys. Rev. B* **1997**, *56*, 1809.
(30) Cava, R. J.; Murphy, D. W.; Zahurak, S.; Santoro, A.; Roth, R. S. *J. Solid State Chem.* **1984**, *53*, 64–75.
(31) Murphy, D. W.; Cava, R. J.; Zahurak, S. M.; Santoro, A. *Solid State Ionics* **1983**, *9−10*, 413–417.
(32) Wagemaker, M.; van de Krol, R.; Kentgens, A. P. M.; van Well, A. A.; Mulder, F. M. *J. Am. Chem. Soc.* **2001**, *123*, 11454–11461.
(33) Kim, J. H.; Myung, S. T.; Sun, Y. K. *Electrochim. Acta* **2004**, *49*, 219–227.
(34) Masarapu, C.; Subramanian, V.; Zhu, H.; Wei, B. *Adv. Funct. Mater.* **2009**, *19*, 1008–1014.